Development of IMARAD CZT Detectors with PIN Contacts

T. Narita[1], P.F. Bloser[1], J.E. Grindlay[1], J.A. Jenkins [1], H.W. Yao[2]

[1]Harvard-Smithsonian Center for Astrophysics, 60 Garden St., Cambridge, MA 02138

[2]Sandia National Laboratories, 7011 East Ave., Livermore, CA 94551

ABSTRACT

We present initial results from our evaluation of a PIN contacted pixellated detector using cadimum zinc telluride substrate produced by IMARAD Imaging Systems. The Horizontal Bridgman (HB) grown crystals from IMARAD have been shown to produce high resolution photopeaks, but they are also seen to have large dark current. We seek to test whether the use of PIN contacts could reduce the dark current and thus improve the spectral response especially in the 10-100 keV energy range. We have fabricated PIN and MIN detectors with a 4×4 array of pixels on 10×10 mm substrates. Measurements of the detectors' dark current, spectral response, and internal electric field are presented and compared to IMARAD's ohmic contact detector and PIN detectors made of HPB material.

Keywords: CdZnTe, PIN, pixellated imaging detectors, hard X-ray imaging

1. INTRODUCTION

In the past several years, Cadmium Zinc Telluride (CZT) has gained a wide acceptance as an important semiconductor for X-ray and gamma-ray detectors. A CZT detector can operate at room temperature due to its large bandgap, and it is free of polarization effects found in CdTe. A variety of electrode designs have been studied to compensate for hole trapping, and one is now able to obtain much better energy resolution than in scintillators. The favorable material properties and advances in readout design have made CZT a promising material in a variety of fields, including astronomy. However, before CZT can fully replace scintillators in large area detectors, the crystal growth process must be refined to reduce cost and increase the yield of large volume spectroscopic grade crystals. Presently, the best method of crystal growth is the High Pressure Bridgman (HPB) technique. HPB grown crystals have resistivities around 10^{11} ohm-cm and they can be relatively free of structual defects. Still, the yield of HPB materials with dimensions greater than 10×10 mm and free of macroscopic defects is low. For applications such as a hard X-ray astronomical survey, where the required detector area is on the order of square meters, the cost of testing and tiling small detectors would be prohibitive.

IMARAD Imaging Systems has recently made available CZT which is grown using a modified Horizontal Bridgman (HB) process.[1] This method can produce defect free crystals of larger dimensions up to 40mm at $\sim 25\%$ yield.[2] A 40×40 mm pixellated detector made with IMARAD CZT has been tested and found to have uniform leakage current and spectral response from pixel to pixel.[2] By using larger crystals, the problems associated with tiling detector modules into a large area array are greatly simplified. However, one drawback of the HB process is that the crystals are typically lower in resistivity than those made with HPB process. A pixellated IMARAD detector which uses indium for the electrodes has a resistivity of around 5×10^9 ohm-cm.[3] While low resistivity is not critical for spectroscopy at X-ray energies greater than 100 keV, the large leakage current significantly degrades the energy resolution at 5-60 keV.

One method to increase the resistivity of a detector, and thus the spectral resolution, is the addition of blocking contacts. PIN blocking contacts have been successfully evaporated onto CZT using a low temperature technique.[4] As a part of our astronomical hard X-ray detector program, we have been working to build pixellated CZT detectors using PIN contacts. We have already shown that addition of CdS and ZnTe as the anode and cathode contacts will modestly improve the resistivity of a HPB CZT detector.[5] A natural extension of this approach is to try the similar blocking contacts on lower resistivity material, such as IMARAD's CZT. In this paper, we report our results from pixellated PIN and Schottky contact detectors made with IMARAD CZT. We measured the detectors for material uniformity, resistivity, and spectral response. We also report on the extent of the depletion layer near the contacts and present results from low temperature tests of the detectors.

Further author information: (Send correspondence to T. Narita)
tnarita@cfa.harvard.edu

IMARAD Sample D-07-103 B:

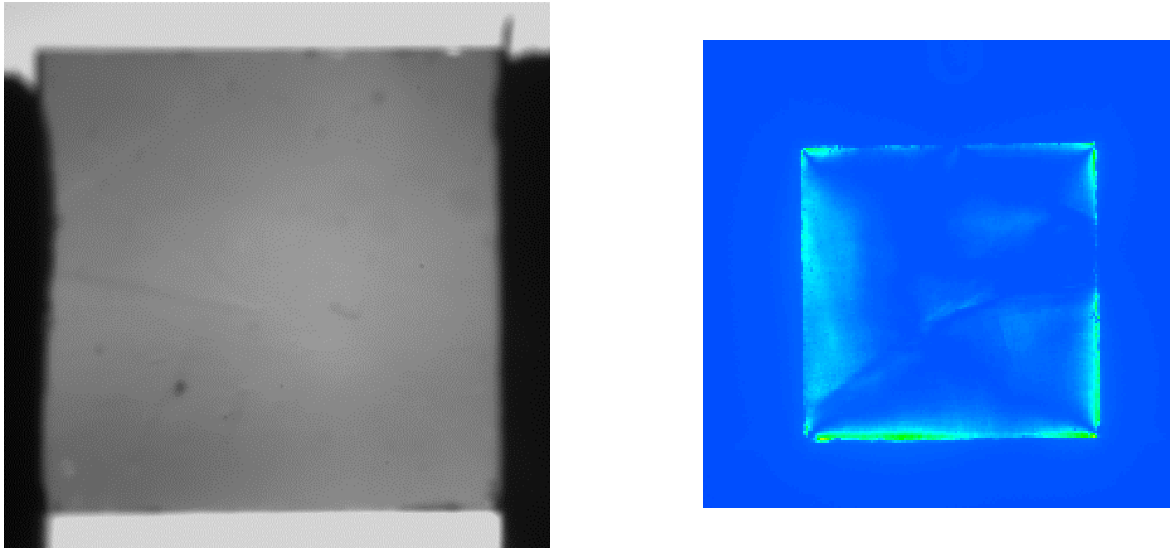

Bright Field **Dark Field**

Figure 1. IR micrograph image (left) and polarized light transmission image (right) of one of the $10 \times 10 \times 4$ mm IMARAD samples (D-07-103) prior to metallization. The sample has no cracks or grain boundaries.

2. PIN DETECTOR DEVELOPMENT

2.1. Material Uniformity and Properties

Infrared (IR) micrograph images of several IMARAD samples were obtained to study the uniformity of the crystals. IR imaging can highlight macroscopic defects in CZT, such as pipes, grain boundaries and cracks. These defects can distort the internal electric field and result in poor carrier mobility.[6] We IR imaged four $10 \times 10 \times 4$ mm samples which were cut from one 20×20 mm sample and a second set of four $10 \times 10 \times 5$ mm samples cut from another large crystal. A representative example from the first set is shown in Figure 1. The same $10 \times 10 \times 4$ mm crystals were also examined by irradiating them with polarized light and observing the transmitted light through an orthogonally polarized filter. In this imaging technique, the depolarized light scattered from a crystal defect appears bright to the viewer while the non-scattered light is absorbed by the filter.

The IR image and the polarized light image show the crystal to be uniform and free of macroscopic defects. No cracks or grain boundaries are seen. The other three crystals in the first set are similarly uniform. There is some light scatter occurring near the crystal edges but this is probably due to the the dicing process, since the internal region remains defect-free. A representative example from the second set is shown in Figure 2. This crystal has diagonal twin lines running across the crystal face but no macroscopic cracks or grain boundaries are seen in the center region of the sample. Small cracks near the edges are probably due to the dicing process. A second crystal from the same batch also showed twin lines but no macroscopic defects were found in any of the other three samples.

Measurement of electron trapping in CZT is an important issue in detector performance. Large values for the charge carrier mobility (μ) and the mean drift time (τ) indicate less trapping and are sought for near complete charge collection. We measured the electron $\mu\tau$ product for a standard IMARAD detector by irradiating the cathode contact with a ^{241}Am source (60 keV) and recording the peak pulse height amplitude value for pulses shaped with 0.5μs time constants at various bias voltage values. By fitting the result with the Hecht relation,[7] we found the $\mu\tau$ product for the IMARAD detector to be $1.55 \times 10^{-3} cm^2 V^{-1}$ (Fig. 3). This value is consistent with published $\mu\tau$ values for HPB grown materials.[6]

2.2. Detectors

We fabricated one PIN and two MIN pixellated detectors from the first set of four $10 \times 10 \times 4$ mm CZT samples from IMARAD. As mentioned above, the four crystals were diced from one 20×20 mm sample. The large crystal was initially contacted with indium pixels and characterized at IMARAD as a working detector. The detectors were processed locally at Spire Corporation (Bedford, MA).

The PIN detector (hereafter called IMARAD ZnTe/CdS) used ZnTe (p-type) for the solid cathode contact and CdS (n-type) for the pixel array. The pixels were 1.5 mm square with 1.7 mm pitch. A 1 mm wide guard ring

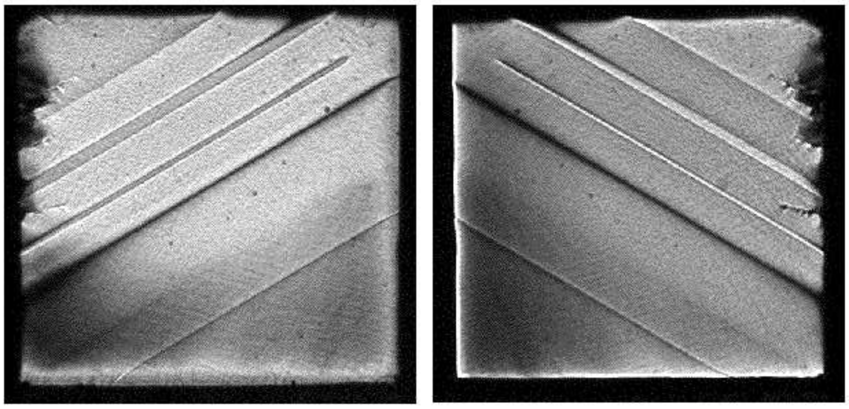

Figure 2. Front and back IR micrograph image of one of the $10 \times 10 \times 5$ mm IMARAD samples. Diagonal twin lines are seen but there are no cracks or grain boundaries.

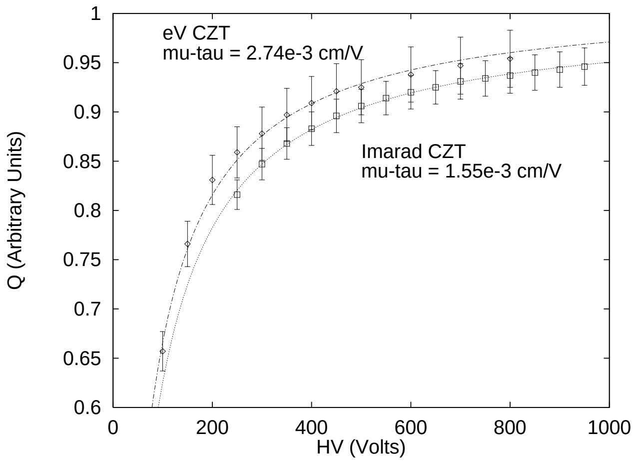

Figure 3. Electron $\mu\tau$ product for standard IMARAD detector is shown. For comparison, we have also plotted the curve for a pixellated MSM detector made with eV Products CZT.

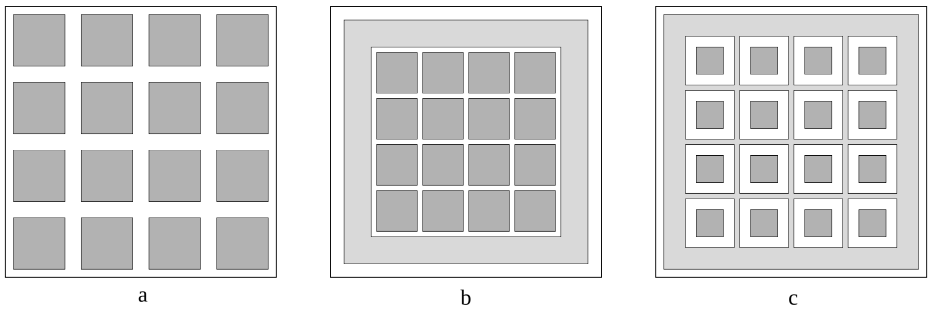

Figure 4. The pixel side layout is sketched for the IMARAD Au/In (a), IMARAD ZnTe/CdS and Au/CdS with 1.5mm pixel (b), and IMARAD Au/CdS with 1.0mm pixel (c).

Detector	Pixel Size	Thickness	Resistivity
IMARAD Standard In/In	1.9mm	4mm	1.1
IMARAD ZnTe/CdS	1.5mm	4mm	1.2
IMARAD Au/CdS	1.5mm	4mm	10
IMARAD Au/CdS	1.0mm	4mm	15.3
IMARAD Au/In	1.9mm	5mm	7.2
eV Products ZnTe/CdS	1.0mm	3mm	15.0

Table 1. Detector contact types (cathode/anode) vs. single pixel reverse bias resistivity, in units of 10^{10} ohm-cm.

surrounded the 4×4 pixel array. The MIN detector (hereafter called IMARAD Au/CdS) had the same pixel array and guard ring dimensions as the IMARAD ZnTe/CdS detector, but we used electroless gold for the cathode and CdS for the pixels. A second MIN detector used 1.0 mm square pixels on 2 mm pitch. In addition, we evaporated a commonly connected gold guard ring grid surrounding each pixel. The width of the guard ring grid was $200\mu m$. The second MIN detector also used electroless gold as the cathode contact and CdS as the anode pixel contacts. While the PIN and the first MIN detectors had indium as the final metal contact, the second MIN detector had platinum evaporated over the indium. This was done to avoid the Au-In interface which we found introduced variable gain effects. All three detectors were surface passivated with a layer of ZnSe.

We also received from IMARAD one standard detector: a $20 \times 20 \times 4$ mm crystal with an array of 8×8 1.9 mm indium contacted pixels on 2.5 mm pitch. The cathode plane also used indium. This standard IMARAD detector was used as baseline comparison for the PIN detectors. Subsequently, we received from IMARAD a 4×4 pixel array detector contacted with gold on the cathode and indium on the anode pixels (hereafter called IMARAD Au/In). This detector used the standard IMARAD pixel size of 1.9 mm at 2.5 mm pitch. Both of these detectors were fitted with an insulated metal band which allowed the edge pixels on the detectors to operate without a guard ring. A sketch of detector pixel layout is shown in Figure 4.

2.3. Leakage Current

Single pixel leakage current was measured on all the detectors as a function of bias voltage and we computed their reverse bias resistivities. We list the resistivities in Table 1. A 3×3 array of spring-loaded pogo pins with conductive rubber tips was used to contact each detector. By grounding the exterior eight pins, we were able to isolate the leakage current to that of one center pixel. We used a Canberra high voltage supply and a Keithley 237 as an ammeter. All measurements were taken in the dark and at room temperature. Figure 5 shows the I-V curves taken from a sample pixel on each of the three PIN detector, and the I-V curve from the standard IMARAD detector. Since the pixel sizes and crystal thickness vary from one detector to the next, the I-V curves alone do not indicate the difference in resistivities. However, one can clearly see the qualitative difference in the current-voltage relation between the detectors.

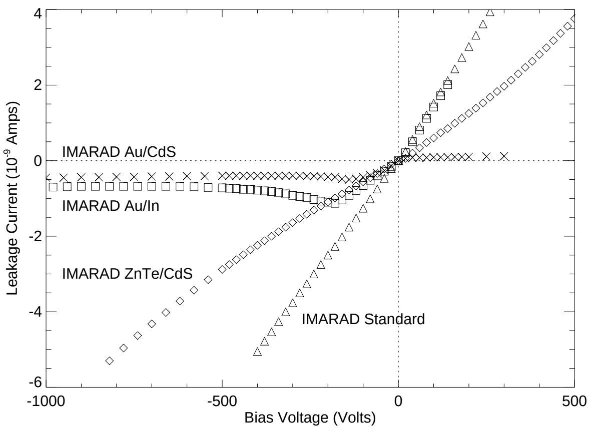

Figure 5. The I-V curves for IMARAD Standard, IMARAD ZnTe/CdS, and IMARAD Au/CdS and IMARAD Au/In detectors are plotted. The gold contacted detectors show diode-like curves and the IMARAD Standard detector shows an ohmic contact curve. The IMARAD ZnTe/CdS detector, despite having p-type and n-type contacts, also shows an ohmic I-V curve.

The IMARAD standard detector and the IMARAD ZnTe/CdS contacted detector both exhibited linear I-V curves. A similar ohmic I-V curve was observed from a gold cathode and gold anode pixellated detector fabricated on eV Products CZT.[8] Since the IMARAD ZnTe/CdS detector used p-type and n-type contacts, the resulting ohmic I-V curve is puzzling.

The IMARAD Au/CdS and IMARAD Au/In detectors both showed diode-like behaviors when reverse biased. When the detectors were forward biased, the IMARAD Au/In detector's current increased linearly but the IMARAD Au/CdS detector's current turned over. A similar forward bias current behavior was observed from our smaller (1.0mm) pixel IMARAD Au/CdS detector. This seems to indicate that a gold contact on IMARAD CZT forms a Schottky barrier while an indium contact on IMARAD CZT forms an ohmic contact. The slight increase in leakage current seen in both detectors at around -100 to -200 V bias is probably due to the bias dependent increase in the conductivity due to the electron transfer effect.

2.4. Energy Resolution

The spectral resolution of the detectors, consisting of photopeak width and photopeak efficiency, was measured at several energies and at various bias voltages. In each case, the test fixture consisted of an array of spring-loaded pins contacting the detector where the outside neighbor pixels were shorted to ground while the center pixel was read out by a low noise eV Products 550 preamp. The preamp output was shaped at 1 μs time constant and recorded by an MCA. Typical single pixel ^{241}Am and ^{57}Co spectra and fits are shown in Figure 6 and Figure 7 for the IMARAD standard, IMARAD Au/CdS and IMARAD In/Au detectors. The detectors were all biased at -700 V. Each spectrum was fit with a HYPERMET function[9] for the photopeak Gaussian and partial charge collection low energy tail. At -700 V bias, the ^{241}Am Gaussian FWHM energy resolutions observed (with no corrections) were 10.0%, 6.0%, and 6.0%, respectively. The photopeak efficiency is defined as the ratio of the counts in the Gaussian to the total counts in the low energy tail and the Gaussian. They were 70%, 74% and 72% in the same order as listed above. Several pixels on each detector were tested and the variation in the energy resolution varied by no more than 1%. The photopeak efficiency also did not vary by more than 3% from pixel to pixel. The Gaussian FWHM energy resolutions of the above detectors at -700 V for w^{57}Co were 4.8%, 3.1% and 3.6%, and the photopeak efficiencies were 62%, 42% and 56%.

The RMS electronic readout noise was measured to be around 200 electrons from a separate pulser test. Once the electronic noise, but not the leakage current noise, was subtracted out in quadrature, the typical detector energy resolution at -700 V bias for ^{241}Am became 9.0%, 3.1% and 3.9%. Longer shaping time would improve the photoelectric charge collection but we found that the IMARAD standard detector's spectrum degrades due to its

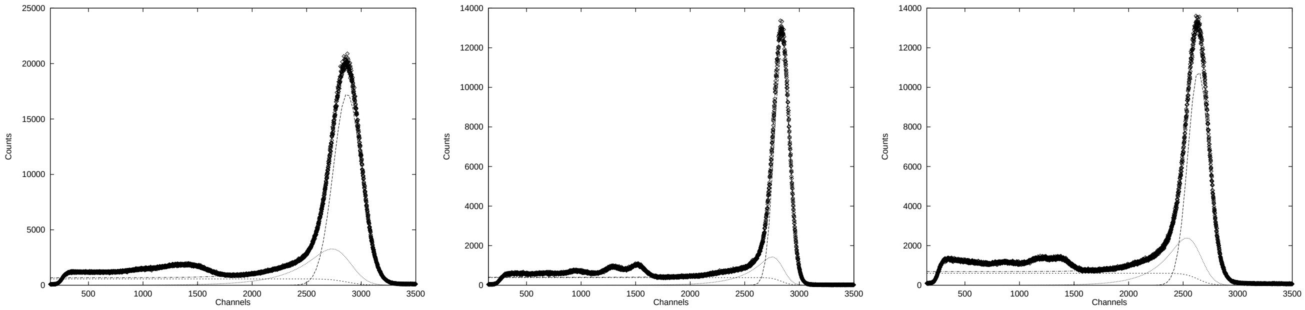

Figure 6. ^{241}Am spectra taken with IMARAD standard, IMARAD Au/CdS and IMARAD In/Au detectors, at -700 V bias. The escapes peaks are resolved in the Au/CdS and In/Au detectors' spectra, indicating a better energy resolution.

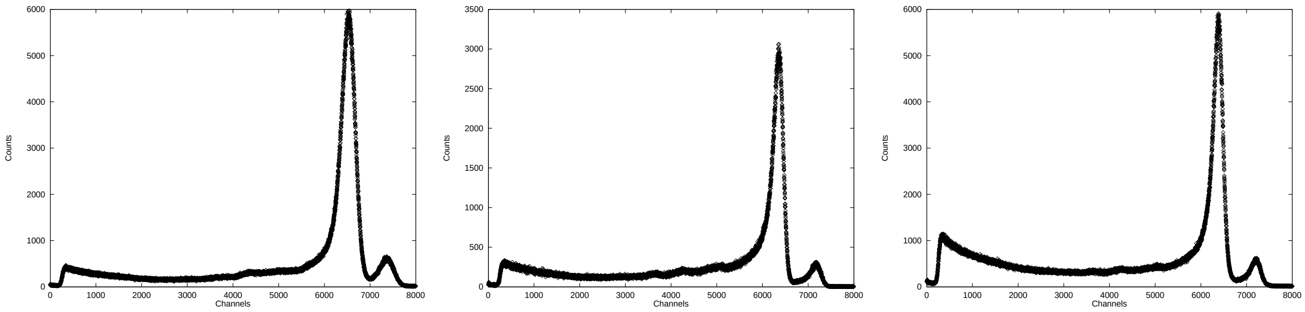

Figure 7. ^{57}Co spectra taken with IMARAD standard, IMARAD Au/CdS and IMARAD In/Au detectors, at -700 V bias.

large leakage current if the shaping time was increased to greater than 2us. From the increase in the peak pulse height channel at longer shaping times, we estimate that with -700 V bias, we are collecting around 85% of the total photoelectric charge with 1 μs shaping time. If we again subtract in quadrature the Poisson statistics variance in the photoelectron charge, we are left with leakage current noise contribution of 445e$^-$, 110e$^-$ and 166e$^-$. The Equivalent Noise Charge (ENC) computed from single pixel I-V curves[10] gave leakage current noise to be 330e$^-$, 70e$^-$ and 140e$^-$, in reasonable agreement with our spectral numbers.

Biasing a detector at higher voltage increases charge carrier mobility and improves the photoelectric charge collection. However, the increase in the leakage current at larger bias may offset the gain or even reduce the spectral quality of the detector. This is a key issue in deciding whether blocking contacts are useful. For each detector, we measured the energy resolutions of the ^{241}Am photopeak at -500, -700 and -1000V, all with 1 μs shaping time. The typical one pixel energy resolution and photopeak efficiency are given in Table 2. One can see the spectral resolution of the CdS/Au and Au/In detectors improves at higher bias. However for the IMARAD standard detector, which shows approximately constant resolution vs. bias, the increased leakage current noise at large bias negates the spectral improvement from better charge collection.

It is worth pointing out that all three detectors have different contacts (ohmic , MIN and Schottky) and small pixel dimensions. The ratio of the pixel size to detector thickness are 0.5, 0.375 and 0.4 in the order listed above. The IMARAD standard detector, despite having the largest small pixel ratio, has the highest ^{57}Co photopeak efficiency (62%). It has been suggested that the ohmic contacts could inject charge carriers and thus improve charge collection.[11] However, when we irradiated the IMARAD standard detector with ^{241}Am from the pixellated anode side, we saw only a very distorted photopeak (Fig 8). This indicates poor hole mobility in the crystal and it seems to contradict the notion of cathode electron injection. Alternatively, the difference in the photopeak efficiency between the detectors might be due to the extent of the depletion region. If a detector with a blocking contact is not fully depleted, the high energy photons events would be subject to poor charge collection, We speculate that the ^{57}Co photpeak efficiencies

Detector	Pixel	Thickness	Bias (V)	FWHM Energy Resolution (^{241}Am)	Pulser Subtracted FWHM Resolution	Photopeak Efficiency
IMARAD Standard	1.9mm	4mm	-500	10.2%	5.8%	54%
			-700	9.8%	4.3%	70%
			-1000	10.5%	2.9%	74%
IMARAD Au/CdS	1.5mm	4mm	-500	6.9%	4.1%	69%
			-700	5.9%	2.9%	74%
			-1000	5.5%	2.3%	86%
IMARAD Au/In	1.9mm	5mm	-500	6.7%	5.0%	68%
			-700	5.8%	3.7%	72%
			-1000	5.0%	2.7%	81%
eV Products ZnTe/CdS	1.0mm	3mm	-600	5.1%	2.4%	73%

Table 2. Average spectral fit parameters as a function of applied bias. When the combined electronic and leakage current noise (pulser) is subtracted out in quadrature, all the detectors show improved energy resolution with increasing bias. However, the raw resolution of the IMARAD standard detector does not improve at higher bias which indicates that this detector is dominated by leakage current noise.

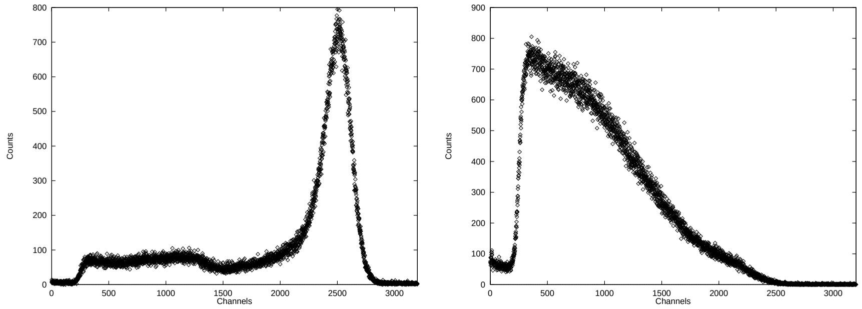

Figure 8. ^{241}Am photopeak when the IMARAD standard detector is irradiated on the cathode plane (left) and on the anode pixels (right). The detector was biased at -500 V. When the detector is irradiated on the anode, the photopeak is severly tailed. This indicates poor hole movement toward the cathode.

of IMARAD Au/CdS and IMARAD Au/In detectors will approach the efficiency of the IMARAD standard detector at higher bias.

2.5. PIN Depletion

For any PIN detector, the active volume is dependent on the size of the depletion layer where the electric field is the strongest. We measured the extent of the depletion layer within our PIN and MIN detectors by directly observing the internal electric field and also comparing the line strength ratio of two different energies of ^{133}Ba.

The direct imaging technique utilizes the electro-optical characteristic of CZT. While CZT is electro-optically isotropic at zero bias, it becomes bi-refringent when a bias voltage is applied. When linearly polarized light enters the material, a phase difference is induced between the light waves travelling parallel and perpendicular to the applied electric field. This causes a rotation of the polarized light, depending on the field strength and the material distance through which the light travels. When the passed light is viewed through an orthogonally polarized filter, the high field region of the crystal appears bright.[12] Figure 9 shows the IMARAD Au/CdS detector viewed using this technique. Although there is some spatial dependence on the extent of the depletion layer, the high field region shown in the false color image clearly increases with larger applied bias.

We also uniformly irradiated our detectors with a ^{133}Ba source and measured the strengths of the 80 keV and the 356 keV lines as a function of the applied bias. The line strength is taken to be the total number of counts in

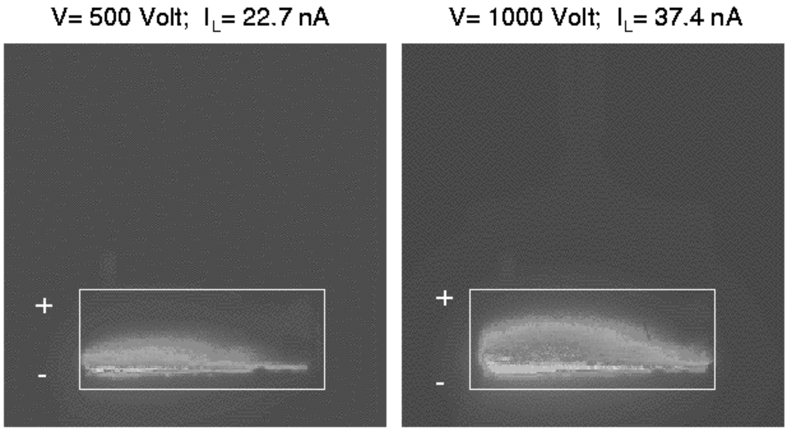

Figure 9. False color image showing the high electric field region within the IMARAD Au/CdS detector as a function of applied bias. The white box outlines the detector and the anode side is marked with a +. The region size appears to vary from one side of the detector to the other.

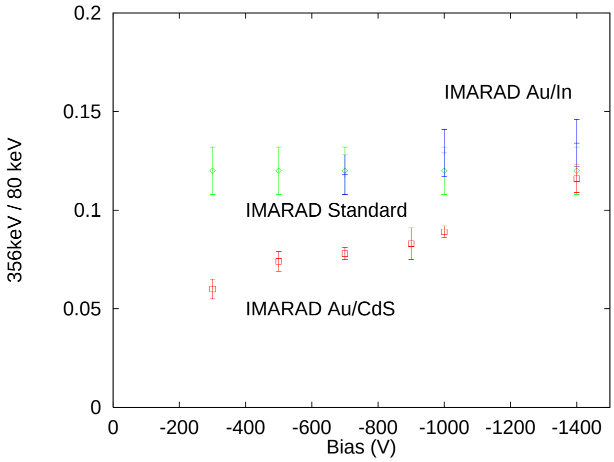

Figure 10. The line strength ratio of ^{133}Ba 356 keV and 80 keV. The line ratio for IMARAD standard detector is constant at $\sim$ 12%. The line ratios for IMARAD Au/CdS and IMARAD Au/In detectors increase with higher applied bias, indicating the internal electric field is becoming more uniform.

the photopeak Gaussian per unit integration time. After correcting for small attenuation caused by the test fixture, we plot the ratio for the IMARAD standard, IMARAD Au/CdS and IMARAD Au/In detectors in Figure 10.

The line ratio for the IMARAD standard detector remains relatively constant at $\sim$ 12% regardless of the applied voltage. Since the internal electric field is presumed to be uniform inside an ohmic contact detector, the constant line ratio is not surprising. However, the line ratios for IMARAD Au/CdS and IMARAD Au/In detectors increase with higher applied voltage, which indicates an increase in their active volume. The three detectors have similar line ratios at 1400 V. We speculate that the IMARAD Au/CdS and IMARAD Au/In detectors are becoming fully depleted at $\sim$ 1500 V.

2.6. Thermal Effects

Since we intend to develop astronomical CZT instruments which could reside outside pressurized containers, we examined the detector performance at sub-zero temperatures. IMARAD standard, IMARAD ZnTe/CdS, IMARAD

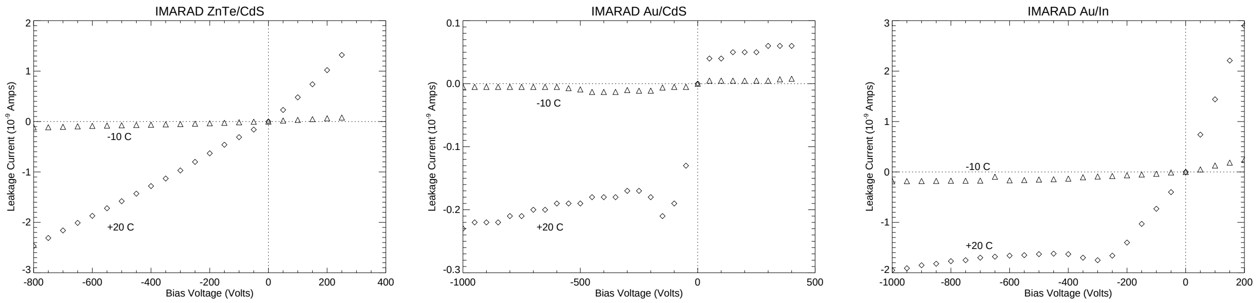

Figure 11. I-V curves of three PIN, MIN and Schottky contacted detectors at +20 and -10 degrees.

Au/CdS and IMARAD Au/In detectors were individually placed in a thermal chamber and cooled down to $-20°$ C. The spring-loaded pin array test fixture and a low noise preamp were also placed inside the chamber. The temperature of the detector was measured by a thermistor attached to the test fixture. To minimize the thermal shock to the CZT, the chamber was controlled such that the temperature slew of the detector fixture was about 0.3 degree per minute.

The temperature dependence of the single pixel leakage current was measured by recording I-V curves at 20, 0, -10 and -20 Celsius. Figure 11 shows the the I-V curve overlays of PIN, MIN and Schottky contacted detectors. The reverse bias resistivity at $-20°$ C for the detectors shown in Figure 11 are 1.3×10^{12}, $> 7 \times 10^{14}$ and 9×10^{11} ohm-cm respectively. This corresponds to a factor of $\times 500$, $> \times 1000$ and $\times 15$ increase in resistivity from 20° C. We note that even at $-20°$ C, the IMARAD ZnTe/CdS detector's IV curve does not roll-over but maintains a linear relationship.

We also examined the spectral performance by recording ^{241}Am spectra while the temperature was varied. Each spectrum was integrated for 20 minutes while the temperature of the detector stayed constant within $\pm 1°$ C. The detectors were all biased at -700 V. Figure 12 shows a mosaic of spectra taken with IMARAD standard, IMARAD Au/CdS and IMARAD Au/In detectors, at 20, -10 and -20 Celsius. There was additional noise from the refrigeration unit which broadened the photopeaks in the spectra. As the temperature cooled below 10°, the photopeak count rate and gain with the IMARAD Au/CdS and IMARAD Au/In detectors decreased, and the photopeak disappeared by -20°. We tested the preamplifier and the conductive rubber individually and ruled out any effects due to electronics or contact problems. We believe this could be caused by a decrease in the depletion depth at lower temperature. Such a change could account for the loss in gain and count rate. Interestingly enough, the photopeak in the IMARAD standard detector became more prominent at -20°, with the number of counts in the photopeak doubling between -10° to -20°. An adjacent pixel also behaved similarly with an increased count rate at -20°. The increase in the count rate at lower temperature is thought to be due to a change in the thin inactive region near the ohmic cathode contact.[3] If the inactive region decreased in size with lower temperature, it would result in an increase in the low energy photon detector volume. We plan to further study the temperature dependent photometry of a IMARAD standard detector using higher energy photons.

3. CONCLUSIONS

A low cost method of growing large volume, uniform quality CZT is needed to realize our goal of building a very large area detector for a hard X-ray survey mission, EXIST.[13] Past methods of crystal growth have yielded a low volume of spectroscopic quality material, which increased the cost and difficulties in making a large tiled detector. IMARAD Imaging Systems has recently made available large volume CZT grown using a modified Horizontal Bridgman process. In this paper, we have characterized several detectors made from CZT samples supplied to us by IMARAD. We found the material to be free of macroscopic defects and the pixellated detectors made with the materials had spatially uniform response and performance. We investigated the addition of blocking contacts on IMARAD CZT and found that detectors made with gold cathode, with either CdS anode or In anode, had substantially higher reverse bias resistivity and improved energy resolution. The depletion layer in the detectors with blocking contacts increased with bias and we infer that a voltage of $\sim$ 1500 V is necessary to fully deplete a 4-5mm detector. We also found that a standard IMARAD detector with ohmic contacts performed better when cooled while the detectors with blocking contacts stopped working when cooled.

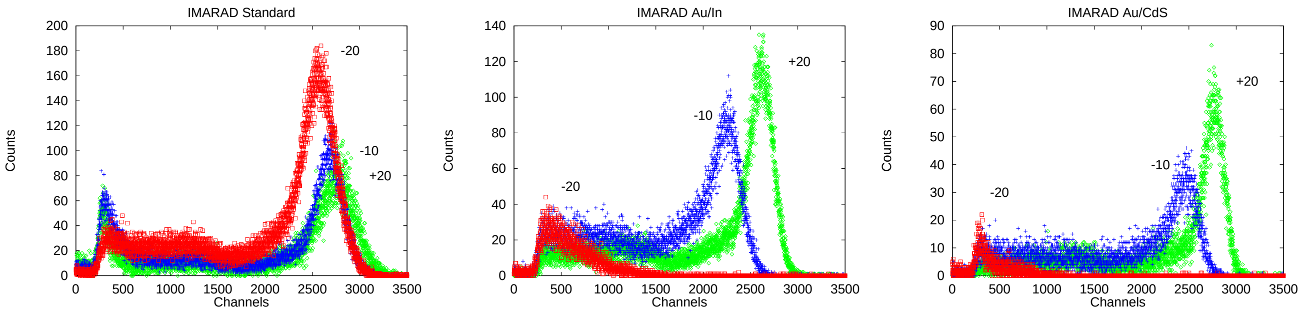

Figure 12. Temperature dependent ^{241}Am spectra taken with IMARAD standard (left), IMARAD Au/In (center) and IMARAD Au/CdS (right) detectors. The IMARAD standard detector has a thin inactive region which decreases in size with lower temperature, and thus the increase in photon collection at -20°. The Schottky contacted detectors stopped working below -12 to -15 degrees.

ACKNOWLEDGMENTS

We thank Dr. Uri El-Hanany of IMARAD Imaging Systems for supplying us with CZT samples. We also thank J. Toney and D. Taylor at Spire Corp. for the PIN contact fabrication. This work was supported in part by NASA grants NAG5-5103 and NAG5-5209.

REFERENCES

1. P. Cheuvart, U. El-Hanany, D. Schneider, and R. Triboulet *J. Crystal Growth* **101**, 1990.
2. T. Schlesinger, B. Brunett, H. Yao, J. VanScyoc, R. James, S. Egarievwe, K. Chattopadhyay, X. Ma, A. Burger, N. Giles, U. El-Hanany, A. Shahar, and A. Tsigelman, "Large Volume Imaging Arrays for Gamma-ray Spectroscopy," *Presented at II-VI Workshop* , 1998.
3. U. El-Hanany *Private Communication* .
4. R. Sudharsanan, G. Vakerlis, and N. Karam, "Fabrication and Characterization of CdZnTe Radiation Detectors with a New PIN Design," *J. Elect. Mat.* **26**, pp. 745–749, 1997.
5. T. Narita, P. Bloser, J. Grindlay, R. Sudharsanan, C. Reiche, and C. Stenstrom, "Development of Prototype Pixellated PIN CdZnTe Detectors," in *Hard X-Ray and Gamma-Ray Detector Physics and Applications*, F. Doty and R. Hoover, eds., *Proc. SPIE* **3446**, p. 218, 1998.
6. C. Szeles and M. Driver, "Growth and Properties of Semi-Insulating CdZnTe for Radiation Detector Applications," in *Hard X-Ray and Gamma-Ray Detector Physics and Applications*, F. Doty and R. Hoover, eds., *Proc. SPIE* **3446**, pp. 2–9, 1998.
7. K. Hecht, "Zum Mechanismus des Lichtelektrischen Primarstromes in Isolierenden Kristallen," *Zeits. Phys* **77**, pp. 235–243, 1932.
8. P. Bloser, J. Grindlay, T. Narita, and F. Harrison, "CdZnTe Background Measurement at Balloon Altitudes with an Active BGO Shield," in *EUV, X-Ray, and Gamma-Ray Instrumentation for Astronomy*, O.H.W.Siegmund and M. Gummin, eds., *Proc. SPIE* **3445**, p. 186, 1998.
9. G. Phillips and K. Marlowe, "Charge Transport in Arrays of Semiconductor Gamma-ray Detectors," *Nucl. Inst. and Methods* **137**, p. 525, 1976.
10. E. Nygard, P. Aspell, P. Jarron, P. Weilhammer, and K. Yoshioka, "CMOS Low Noise Ampliefer for Microstrip Readout Design and Results," *Nucl. Inst. Meth. A* **301**, pp. 506–516, 1991.
11. U. Lachish, "The Role of Contacts in Semiconductor Gamma Radiation detectors," *Nucl. Inst. Meth. A* **403**, pp. 417–424, 1998.
12. H. Yao, R. Anderson, R. James, and R. Olsen, "Optical Studies of the Internal Electric-field Distributions of CdZnTe Detectors under Bias Conditions," in *Semiconductors for Room-Temperature Radiation Detector Applications II*, R. James, T. Schlesinger, P. Siffert, M. Cuzin, M. Squillante, and W. Dusi, eds., *Proc. MRS* **487**, p. 59, 1998.

13. J.Grindlay, T. Prince, N. Gehrels, J. Tueller, C. Hailey, B. Ramsey, M. Weisskopf, P. Ubertini, and G. Skinner, "Energetic X-ray Imaging Survey Telescope (EXIST)," in *Hard X-Ray and Gamma-Ray Detector Physics and Applications*, *Proc. SPIE* **2518**, p. 202, 1995.